

# A Learning Framework for An Accurate Prediction of Rainfall Rates

Hamidreza Ghasemi Damavandi and Reepal Shah

Future H2O, Office of Knowledge Enterprise Development, Arizona State University, Tempe, AZ, US

## I. ABSTRACT

The present work is aimed to examine the potential of advanced machine learning strategies to predict the monthly rainfall (precipitation) for the Indus Basin, using climatological variables such as air temperature, geo-potential height, relative humidity and elevation. In this work, the focus is on thirteen geographical locations, called index points, within the basin. Arguably, not all of the hydrological components are relevant to the precipitation rate, and therefore, need to be filtered out, leading to a lower-dimensional feature space. Towards this goal, we adopted the gradient boosting method to extract the most contributive features for precipitation rate prediction. Five state-of-the-art machine learning methods have then been trained where pearson correlation coefficient and mean absolute error have been reported as the prediction performance criteria. The Random Forest regression model outperformed the other regression models achieving the maximum pearson correlation coefficient and minimum mean absolute error for most of the index points. Our results suggest the relative humidity (for pressure levels of 300 mb and 150 mb, respectively), the u-direction wind (for pressure level of 700 mb), air temperature (for pressure levels of 150 mb and 10 mb, respectively) as the top five influencing features for accurate forecasting the precipitation rate.

### *Keywords:*

Artificial Neural Networks (ANNs), Gradient Boosting feature extraction, Indus Basin, Precipitation rate, Random Forest

## II. INTRODUCTION

Precipitation rate is a crucial concern for food production plan and water resource management. The prolonged dry period or heavy rain at the critical stages of the growth may lead to significant reduce crop yield. Additionally, accurate precipitation prediction could serve to alert the early warnings of sever weather events. Numerical prediction of precipitation rate has long been beneficial but a complex task for meteorologists, as it depends on other factors such as surface temperature (ST), humidity which often fluctuate in time and space. Hence, developing rigorous mathematical methods to accurately forecast the precipitation rate is of paramount importance. The motive is to harness the methodologies offered in data mining and machine learning fields to explore the other hydrological components in order to devulge valid and potentially useful internal relationships of these components as

probable predictors to forecast the precipitation rate. Establishment of a machine learning model for precipitation prediction is rife with statistical assumptions to fine-tune the model's hyper-parameters, and hence, reduce the computational time complexity and boost the prediction accuracy. Therefore, the artificial intelligence strategies can be considered as a highly efficient replacement for the traditional physical-based hydrological models. Several studies have focused on the implementation of machine learning techniques in precipitation prediction. Sumi et. al. 2012 [1] investigated the potential of the artificial neural network, multivariate adaptive regression splines, the k-nearest neighbour, and radial basis support vector regression for daily and monthly rainfall prediction of Fukuoka city in Japan. Hybrid models such as the combination of wavelet transform and artificial neural network (WANN) has been proposed by Kim et.al 2003 [2] where predictive models to predict the Conchos River Basin were proposed and evaluated. Karran et .al 2014 [3] compared the use of four different models, i.e. ANN, SVR, waveletANN, and wavelet-SVR in a Mediterranean, Oceanic, and Hemiboreal watershed. Khan et.al 2006 [4] examined the potential of Support Vector Regression (SVR) and Multilayer Linear Perception (MLP) in predicting lake water levels. Specifically, water level data for Lake Erie from 1918 to 2001 were used in training the two models to predict this property for the following 12 months; although the evaluation results (using root-mean-square and correlation coefficient) were promising in both cases, the intra-model comparison showed that the MLP outperformed SVR. Figure 1 illustrates the process to forecast the precipitation rate for the region of interest. We work out our precipitation on a index point by index point basis. For each index point, the precipitation rate is passed through the "Feature Selection" module where the most contributive predictors are determined. We withhold 90% of the data for training the learning model and use the remaining 10% for the evaluation. The optimal hyper-parameters are learned in the "Model Training" module and the performance of the model is evaluated by pearson correlation coefficient and mean absolute prediction error for the testing data in the "Model Evaluation" module.

The rest of the paper is organized as follows. Section III explains the region of the study and the dataset used in this work. The problem formulation and the methodology for extracting the informative features fore precipitation prediction are presented in Section IV. The most contibutive features as well as the performance of each learning model is illustrated in the Section V. Section VI concludes the paper.

We used precipitation data from 0.05 degree (5.528 Km)

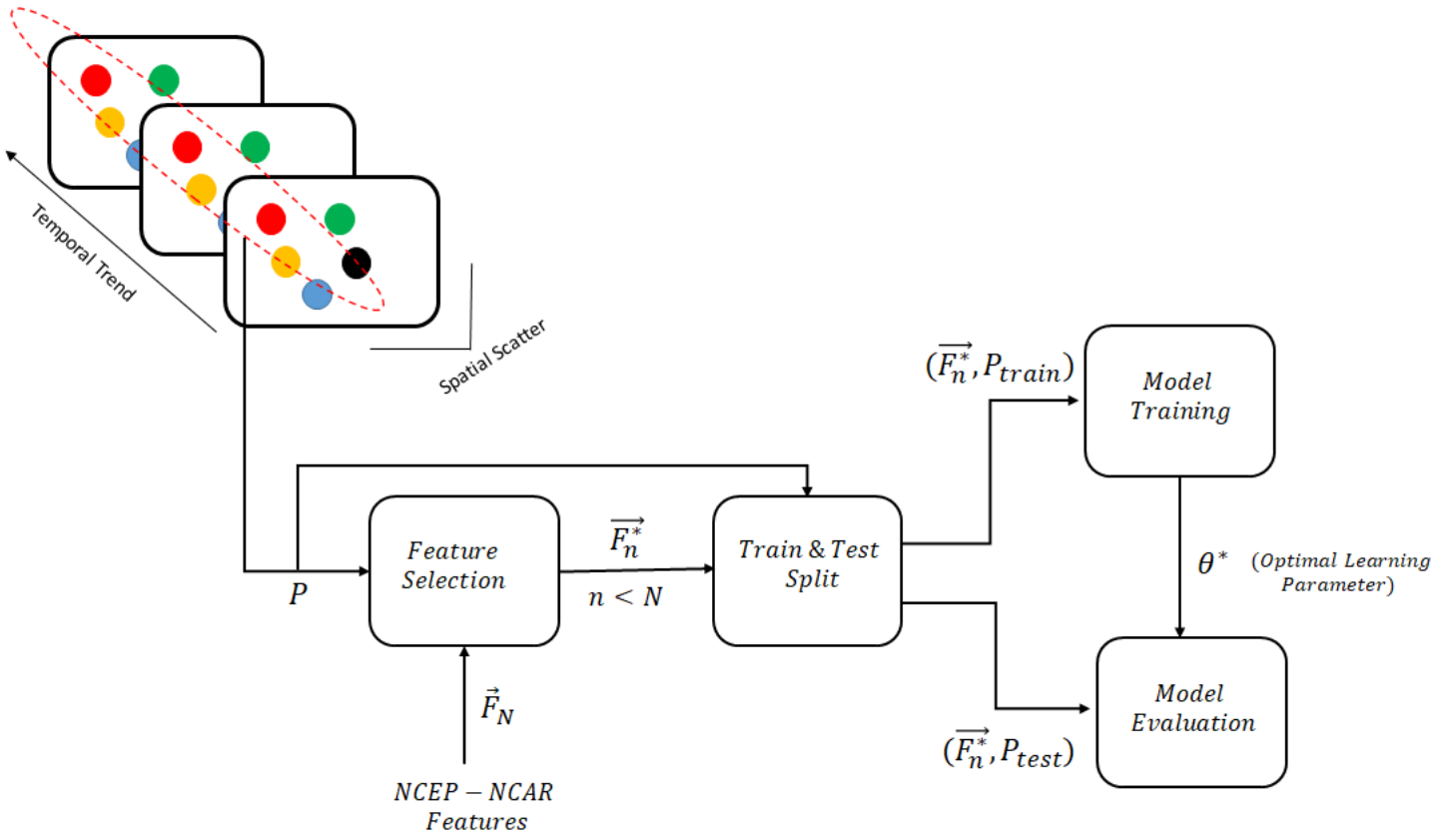


Fig. 1: The block diagram of the precipitation rate prediction procedure via NCEP-NCAR features.

Climate Hazards Group InfraRed Precipitation with Station data (CHIRPS) v2 product. This product was developed by Funk et al. 2015 [5] by merging station-based data with satellite-based data. Initially global climatological mean was developed using station-based data from Food and Agricultural Organization (FAO) and Global Historical Climate Network (GHCN). This in total accounts for the total observations of  $\sim 50,000$  stations across globe. Long-range precipitation derivatives were derived from Thermal Infra Red (TRI) Cold Cloud Duration (CCD) observation. Based on this two dataset, precipitation estimates were derived, named as CHRIP. Further, they merge station-based data from 2,00,000 locations from five different sources, generally observations decline from 32000 in 1980 to less than 14000 in 2014. This product is called CHIRPS. We took air temperature (Air), Geopotential height (Hgt), Relative humidity (Rhum), Specific humidity (Shum), Sea level pressure (Slp), u and v- direction wind as the potential predictors of the precipitation. The predictors were taken from NCEP-NCAR Reanalysis from 1981 to 2017 (37 years). Atmospheric variables in NCEP-NCAR reanalysis are simulated by assimilating station-based observation. Variables from NCEP-NCAR reanalysis were available at 2.5 degree. Hence precipitation from CHIRPS was aggregated for 2.5 degree resolution. Note that, these predictors were capture for different pressure levels (up to seventeen pressure levels) indicated in Table I. To be clear, two measured values for relative humidity at two different pressure levels are considered two unique potential predictors. Our constructed database

would then consists of eighty-five unique predictors and their corresponding precipitation rate. These seventeen pressure levels (milli-bars) are 1000, 925, 850, 700, 600, 500, 400, 300, 250, 200, 150, 100, 70, 50, 30, 20 and 10. For simplicity, throughout this paper, we show these levels by  $l_1$  to  $l_{17}$ . With this in mind, air temperature measured at first layer (1000 mb), would be represented as  $ar^{l_1}$ .

### III. REGION OF INTEREST

The Indus basin with the total area of 1.12 million  $km^2$  ( $432434.4176 mi^2$ ) touches 4 countries of China (8 percent), India (39 percent), Afghanistan (6 percent) and Pakistan (47 percent). The Indus river originates from Lake Ngangla Ring Tsho in Tibetan plateau in the north, extending south to the dry plains in Pakistan and finally flows into the Arabian Sea. The rainfall in this basin is negligible and the snow and glaciers of the Hindu Kush - Himalayas and seasonal monsoon rains (July to September) are considered the main water input to this basin. Being considered as the main source of water for agriculture, industrial productions, and human consumption, Indus basin Irrigates more than 30 million hectares of agricultural land in the basin through 15 tributaries including the Ravi, Beas, and Sutlej rivers in India, the Swat, Chitral, and Chenab rivers in Pakistan and Kabul River in Afghanistan. Hence, Indus river is considered as the vital water resource of the region.

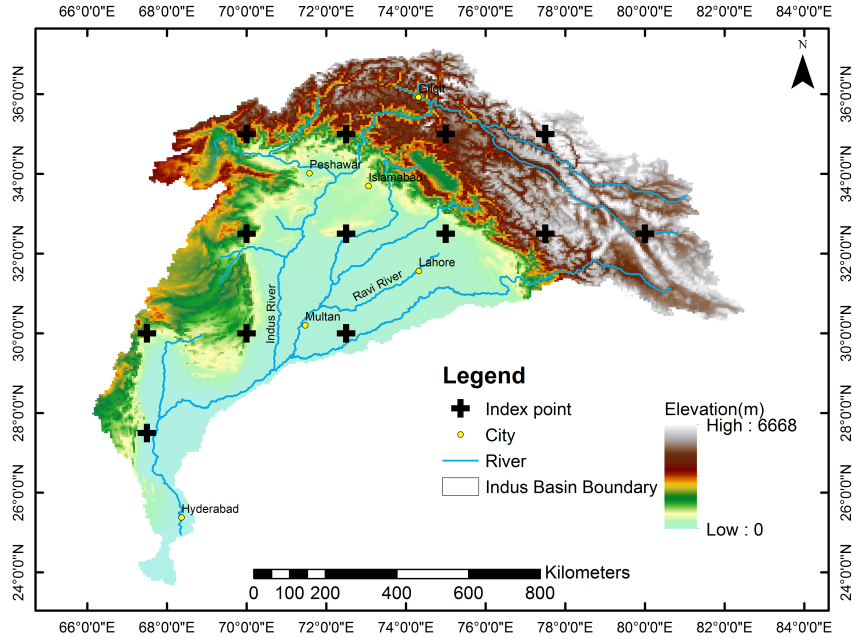


Fig. 2: Indus basin: Region of Interest

#### A. Dataset

We used precipitation data from 0.05 degree (5.528 Km) Climate Hazards Group InfraRed Precipitation with Station data (CHIRPS) v2 product. This product was developed by Funk et al. 2015 [5] by merging station-based data with satellite-based data. Initially global climatological mean was developed using station-based data from Food and Agricultural Organization (FAO) and Global Historical Climate Network (GHCN). This in total accounts for the total observations of  $\sim 50,000$  stations across globe. Long-range precipitation derivatives were derived from Thermal Infra Red (TRI) Cold Cloud Duration (CCD) observation. Based on this two dataset, precipitation estimates were derived, named as CHRIP. Further, they merge station-based data from 2,00,000 locations from five different sources, generally observations decline from 32000 in 1980 to less than 14000 in 2014. This product is called CHIRPS. We took air temperature (Air), Geopotential height (Hgt), Relative humidity (Rhum), Specific humidity (Shum), Sea level pressure (Slp), u and v- direction wind as the potential predictors of the precipitation. The predictors were taken from NCEP-NCAR Reanalysis from 1981 to 2017 (37 years). Atmospheric variables in NCEP-NCAR reanalysis are simulated by assimilating station-based observation. Variables from NCEP-NCAR reanalysis were available at 2.5 degree. Hence precipitation from CHIRPS was aggregated for 2.5 degree resolution. Note that, these predictors were capture for different pressure levels (up to seventeen pressure levels) indicated in Table I. To be clear, two measured values for relative humidity at two different pressure levels are considered two unique potential predictors. Our constructed database would then consists of eighty-five unique predictors and their corresponding precipitation rate. These seventeen pressure levels (milli-bars) are 1000, 925, 850, 700, 600, 500, 400, 300, 250, 200, 150, 100, 70, 50, 30, 20 and 10. For simplicity,

throughout this paper, we show these levels by  $l_1$  to  $l_{17}$ . With this in mind, air temperature measured at first layer (1000 mb), would be represented as  $ar^{l_1}$ .

## IV. METHODOLOGY

#### A. Problem Statement

We attempt to predict the precipitation rate at an index point  $\vec{l} = (lon, lat, elev)$  at time  $t$  via other hydrological components such as air temperature, relative humidity .etc. It's noteworthy that, each layer within a hydrological component would also be treated as a potential predictor. In this work, we try to extract a subset of relevant features which can efficiently describe the input data while reducing effects from noise or irrelevant variables and still provide promising prediction results. Specifically, we focus on gradient boosting method, expatiated in Section IV-B2. Technically, we attempt to derive a function like  $G(\cdot)$  to map the relevant observed variables (denoted in Table I) for a specific geographical location  $\vec{l}$  and sometime  $t$  into a precipitation rate, deviated by some noise level of  $w(\cdot)$ .

$$P(\vec{l}, t) = G(\vec{F}(\vec{l}, t)) + w(\vec{l}, t) \quad (1)$$

Towards this goal, five state-of-the-art learning models are trained on a location by location basis.

#### B. Feature Selection

Our dataset consists of  $M$  examples (the monthly reported components of index points for Indus basin across the thirty-seven years) and  $N$  potential predictors to forecast the precipitation rate ( $M$  and  $N$  equal to 5772 and 85, respectively). We focus on extracting the top  $\kappa$  (here  $\kappa$  is ten) most contributive predictors to forecast the precipitation rate.

1) *Removing Linearly Correlated Features*: For any two potential predictors with the size of the example i.e.  $M$ , namely  $f_i^M$  and  $f_j^M$ , we examine their linear correlation via the cosine angle between them in the feature space:

$$\cos(\phi_{i-j}) = \frac{\langle f_i, f_j \rangle}{|f_i|_1 \cdot |f_j|_1} \quad (2)$$

where  $\langle \cdot \rangle$  and  $|\cdot|_1$  determine the inner product and the  $L_1$  norm, respectively. We call two predictors, "co-linear" variables, if the above-mentioned  $|\cos(\cdot)|$  is at least  $\gamma$  (here  $\gamma = 0.9$ ). In the first phase of feature filtering procedure, we remove the highly correlated predictors.

2) *Selecting Optimal Features of Predictive Model*: As the next stage to filter out the irrelevant features, we exploit the gradient boosting method. Gradient boosting is a machine learning technique for regression problem, which produces a prediction model in the form of an ensemble of weak prediction models, typically decision trees. Given the dataset of size  $K$ ,  $\{y_i, x_i\}_{i=1}^{i=K}$ , we attempt to fit a model  $F_m(x)$  to minimize the square loss at the  $m^{\text{th}}$  stage of the algorithm. Such imperfect model, or the so-called weak model, would lead into some non-zero regression error. We now add an additional model  $h$  to  $F$  towards reducing this regression error, and hence the new model would be  $F_{m+1}(x) = F_m(x) + h(x)$ . Such new model would ideally be chosen to lead into a zero regression error, or  $F_{m+1}(x_i) = F_m(x_i) + h(x_i) = y_i \forall 1 \leq i \leq K$  or equivalently  $h(x_i) = y_i - F_m(x_i)$ . In other words, in each stage, we add a new model  $h(\cdot)$  to the existing model to compensate its shortcomings, or the regression error.  $y_i - F_m(x_i) \forall 1 \leq i \leq K$  are called the residuals. Now towards identifying such  $h(\cdot)$  model, we would fit a curve to the residuals, i.e. fit a curve to the data set  $\{y_i - F_m(x_i); x_i\}_{i=1}^{i=K}$ . Such fitted curve would then be added to construct  $F_{m+1}(x)$ . Obviously this new model is a stronger model with respect to  $F_m(x)$  leading to a lower regression error. In case the regression error with the new model ( $F_{m+1}(x)$ ) is still unsatisfactory, we would construct  $F_{m+2}(x)$  via adding a new  $h(x)$  to  $F_{m+1}(x)$  with the same previous procedure.

We now show that this idea is equivalent to updating the model using the gradient descent. Consider the dataset  $\{y_i; F(x_i)\}_{i=1}^{i=K}$  with an attempt to minimize the square loss of  $J = L(y, F(x)) = \sum_{i=1}^K [\frac{1}{2}(y_i - F(x_i))^2]$ . The gradient descent of  $y$  with respect to  $F(x)$  is:

$$\frac{\partial J}{\partial F(x_i)} = \frac{\partial \sum_{i=1}^K [\frac{1}{2}(y_i - F(x_i))^2]}{\partial F(x_i)} = F(x_i) - y_i = -h(x_i) \quad (3)$$

and the model at  $(m+1)^{\text{th}}$  stage is:

$$F_{m+1}(x_i) = F_m(x_i) - \rho \nabla J_{F_m(x_i)} = F_m(x_i) + h(x_i) \quad (4)$$

$$\forall 1 \leq i \leq K, \rho = 1$$

We fine-tune the trained model  $F(x)$  using Equation 4 until the regression error is desirably low. Note that at each stage  $m$ , we construct 100 regression trees and for each input  $x_i$ ,  $F(x_i)$  would be the average regressed values of all of these trees. It is noteworthy to mention that each tree would adopt a subset

of the features to regress the input. We rank the importance of the features in terms of the *number of occurrence* in each of the regression trees. Hence, features will be sorted in terms of contribution to reach the minimum regression error. We acquire the top 10 contributive features and pass on to the learning phase.

| Index | Feature Name                | Pressure Levels (Millibars) |
|-------|-----------------------------|-----------------------------|
| 1-17  | Air for 17 pressure layers  | $l_1$ to $l_{17}$           |
| 18-34 | Hgt for 17 pressure layers  | $l_1$ to $l_{17}$           |
| 35-42 | Rhum for 8 pressure levels  | $l_1$ to $l_8$              |
| 43-50 | Shum for 8 pressure levels  | $l_1$ to $l_8$              |
| 51    | Slp for one pressure level  | $l_1$                       |
| 52-68 | uwnd for 17 pressure levels | $l_1$ to $l_{17}$           |
| 69-85 | vwnd for 17 pressure levels | $l_1$ to $l_{17}$           |

TABLE I: Hydrological features used to predict the precipitation rate.

### C. Models

Five state-of-the-art machine learning models, coupled by the gradient boosting feature selection technique, have been trained and their performance have been reported individually. We examined linear regression, K-nearest neighborhood regression ( $K = 3$ ), random forest, support vector regression and multilayer perception as the predictive model.

## V. RESULT

Let  $P(\vec{l}, t)$  and  $\tilde{P}(\vec{l}, t)$  be the actual and the predicted precipitation rate at a particular geographical location ( $lon, lat, elev$ ) at sometime  $t$ . We evaluate the performance of the predictive learning model via the pearson correlation coefficient ( $\rho$ ) (Equation 5) between the actual and predicted rates, mean absolute prediction error ( $\mu$ ) (Equation 6) and its standard deviation ( $\sigma$ ). Table II represents these parameters for each of the geographical location examined in this work for five different learning models, i.e., Random Forests (RF), K-nearest Neighborhood Regression ( $K$ -NN), Support Vector Regression (SVR), Linear Regression (LR), Multi-linear Perceptron (MLP). It is noteworthy to mention that for each geographical location we have used 90% of the 37 years data and have evaluated the learning model against the remaining 10% datapoints.

$$\rho(\vec{l}) = \frac{cov[P(\vec{l}), \tilde{P}(\vec{l})]}{\sigma_P \cdot \sigma_{\tilde{P}}}, \quad |\rho(\cdot)| \leq 1 \quad (5)$$

$$\mu(\vec{l}) = \frac{\sum_{t=1}^N |P(\vec{l}, t) - \tilde{P}(\vec{l}, t)|_1}{N} \quad (6)$$

Where  $|\cdot|$  represents the absolute value. Table II summarizes the correlation between the predicted and observed values as well as the mean absolute prediction error. As shown, the correlation coefficient ranges from 0.53 in the last index point to 0.93 in the six-th index point. As can be seen here, Random Forest model outperformed the other models, nominated as best predictive model for six of the index points. Note that, these predicted values were calculated just by the internal

relation among the hydrological models, computed in order of seconds, but could achieve the correlation coefficient of up to 0.93. This is an indicative of the potential of the learning models to emulate the complex equations governing the relationship between these components. Table III illustrates the top ten contributive features for each of the geographical region. Table IV represents the number of occurrence of each of the features as the top ten contributive features. According to this table,  $rh^{l1}$  turned out to be the most frequent feature followed by  $rh^{ls}$ ,  $uw^{l4}$ ,  $ar^{l11}$  and  $ar^{l17}$  as the top five feature playing pivotal role in the precipitation prediction. Due to the strong correlation between humidity and precipitation rate, it is of no surprise to determine the relative humidity as the most contributive feature for precipitation rate. We infer this observation by the direct correlation between the air temperature and humidity to the precipitation rate [6] as the humidity can be considered as both the precursor and the result of rain. Our results indicating the importance of wind speed for precipitation rate aligns with some the established prior work e.g. [7], [8] and [9].

## VI. CONCLUSION

Motivated by the recent advances in data-driven models across miscellaneous areas such as environmental and [10], [11] and hydrological sciences [1], as a powerful tool to approximate the physical-based models, this study aimed to evaluate the performance of the artificial intelligence (AI) data-driven models, and in particular, the top state-of-the-art machine learning models to predict the precipitation rate using using other hydrological components listed in Table I over the region of interest i.e. Indus Basin. We reported the prediction performance as the pearson correlation coefficient and mean square error (MAE defined in Equation 6) between the observed and predicted precipitation rates. Random forest model outperformed the others, achieving the maximum pearson coefficient and minimum mean absolute error for most of the index points. We used seven unique hydrological components shown in Table I, each measured in different pressure levels. We treated a component measured at particular pressure level as an individual feature leading to eighty-five distinct potential predictors to forecast the precipitation rate. We harnessed the gradient boosting strategy to extract the relevant features to an accurate prediction. The results reveal the importance of relative humidity, u-direction of wind and air temperature as the prominent predictors to estimate the precipitation rate. The promising results in this work certify the prominent opportunities provided by the artificial intelligence (AI) methods, and particularly machine learning models, to mine the underlying concealed knowledge between diverse hydrological components which is otherwise not readily accessible to the researchers. Although the conventional hydrological models have been well-established but suffer from some shortcomings such as the tedious computational time or the uncertainties in variables estimate. The AI methods have been proven to be effective in tackling these deficiencies while being backed by advanced theories in optimization, and hence, offering efficient alternative for the conventional physical-based hydrological models.

## ACKNOWLEDGMENT

This work was supported by the National Science Foundation award (grant: GRI0458) and conducted at Future H2O, Office of Knowledge Enterprise Development (OKED) at Arizona State University.

## REFERENCES

- [1] S Monira Sumi, M Faisal Zaman, and Hideo Hirose. A rainfall forecasting method using machine learning models and its application to the fukuoka city case. *International Journal of Applied Mathematics and Computer Science*, 22(4):841–854, 2012.
- [2] Tae-Woong Kim, Juan B Valdés, and Javier Aparicio. Frequency and spatial characteristics of droughts in the conchos river basin, mexico. *Water International*, 27(3):420–430, 2002.
- [3] Daniel J Karran, Efrat Morin, and Jan Adamowski. Multi-step stream-flow forecasting using data-driven non-linear methods in contrasting climate regimes. *Journal of Hydroinformatics*, 16(3):671–689, 2014.
- [4] Mohammad Sajjad Khan and Paulin Coulibaly. Application of support vector machine in lake water level prediction. *Journal of Hydrologic Engineering*, 11(3):199–205, 2006.
- [5] Chris Funk, Pete Peterson, Martin Landsfeld, Diego Pedreros, James Verdin, Shraddhanand Shukla, Gregory Husak, James Rowland, Laura Harrison, Andrew Hoell, et al. The climate hazards infrared precipitation with stations—a new environmental record for monitoring extremes. *Scientific data*, 2:150066, 2015.
- [6] Christopher S Bretherton, Matthew E Peters, and Larissa E Back. Relationships between water vapor path and precipitation over the tropical oceans. *Journal of climate*, 17(7):1517–1528, 2004.
- [7] Sen-Hsiung Hsu and Yuh-Lin Guo. Effect of wind speed on the measurement of rainfall. *Crop, Environment & Bioinformatics*, 2(1):81–86, 2005.
- [8] Larissa E Back and Christopher S Bretherton. The relationship between wind speed and precipitation in the pacific itcz. *Journal of climate*, 18(20):4317–4328, 2005.
- [9] Barbro Johansson and Deliang Chen. The influence of wind and topography on precipitation distribution in sweden: Statistical analysis and modelling. *International Journal of Climatology*, 23(12):1523–1535, 2003.
- [10] Hamidreza Ghasemi Damavandi, Ananya Sen Gupta, Robert K Nelson, and Christopher M Reddy. Interpreting comprehensive two-dimensional gas chromatography using peak topography maps with application to petroleum forensics. *Chemistry Central Journal*, 10(1):75, 2016.
- [11] Hamidreza Ghasemi Damavandi, Ananya Sen Gupta, Guadalupe Canahuate, Christopher M Reddy, and Robert Nelson. Robust oil-spill forensics and petroleum source differentiation using quantized peak topography maps. *arXiv preprint arXiv:1807.07484*, 2018.

| Coordinate (longitude, latitude, elevation) | Learning Model | Pearson Coeff. ( $\rho$ ) | MAE ( $\mu$ ) | STD ( $\sigma$ ) |
|---|----------------|---------------------------|---------------|------------------|
| (27.5 , 67.5 , 472.9)                       | RF             | 0.89                      | 3.59          | 3.34             |
|   | K-NN           | 0.87                      | 3.74          | 3.84             |
|   | SVR            | 0.47                      | 5.34          | 7.92             |
|   | LR             | 0.88                      | 3.85          | 3.29             |
|   | MLP            | <b>0.91</b>               | 3.7           | 2.89             |
| (30. , 67.5 , 1232.5)                       | RF             | <b>0.8</b>                | 6.06          | 5.68             |
|   | K-NN           | 0.75                      | 6.25          | 6.49             |
|   | SVR            | 0.39                      | 9.09          | 9.47             |
|   | LR             | 0.77                      | 6.56          | 5.64             |
|   | MLP            | 0.75                      | 7.01          | 5.67             |
| (30. , 70. , 721.5)                         | RF             | <b>0.88</b>               | 8.46          | 7.97             |
|   | K-NN           | 0.87                      | 6.73          | 8.63             |
|   | SVR            | 0.57                      | 12.11         | 16.16            |
|   | LR             | 0.83                      | 8.96          | 8.01             |
|   | MLP            | 0.87                      | 8.15          | 7.05             |
| (30. , 72.5 , 148.2)                        | RF             | 0.88                      | 8             | 7.86             |
|   | K-NN           | 0.76                      | 10.27         | 10.66            |
|   | SVR            | 0.46                      | 14.75         | 16.95            |
|   | LR             | <b>0.89</b>               | 8.55          | 6.15             |
|   | MLP            | -0.64                     | 68.17         | 24.49            |
| (32.5 , 70. , 1203.)                        | RF             | <b>0.9</b>                | 8.36          | 7.14             |
|   | K-NN           | 0.73                      | 11.28         | 10.38            |
|   | SVR            | 0.7                       | 13.64         | 13.28            |
|   | LR             | 0.8                       | 11.45         | 6.51             |
|   | MLP            | 0.73                      | 15.24         | 10.1             |
| (32.5 , 72.5, 326.4)                        | RF             | 0.85                      | 18.81         | 18.34            |
|   | K-NN           | <b>0.93</b>               | 12.85         | 12.62            |
|   | SVR            | 0.65                      | 27.17         | 34.21            |
|   | LR             | 0.8                       | 21.52         | 19.05            |
|   | MLP            | 0.82                      | 20.75         | 17.51            |
| (32.5, 75., 967.7)                          | RF             | <b>0.79</b>               | 34.89         | 44.33            |
|   | K-NN           | 0.71                      | 36.83         | 51.79            |
|   | SVR            | 0.18                      | 49.02         | 80.93            |
|   | LR             | 0.77                      | 40.25         | 42.91            |
|   | MLP            | 0.34                      | 73.55         | 89.66            |
| (32.5, 77.5, 4044.4)                        | RF             | 0.63                      | 27.89         | 24.42            |
|   | K-NN           | <b>0.66</b>               | 25.57         | 22.99            |
|   | SVR            | 0.29                      | 28.12         | 37.43            |
|   | LR             | 0.6                       | 32.7          | 19.94            |
|   | MLP            | -0.27                     | 304.86        | 46.9             |
| (32.5, 80., 4882.1)                         | RF             | 0.68                      | 11.23         | 9.85             |
|   | K-NN           | 0.48                      | 13.36         | 14.17            |
|   | SVR            | <b>0.68</b>               | 12.74         | 14.73            |
|   | LR             | 0.61                      | 12.23         | 10.13            |
|   | MLP            | 0.26                      | 120.48        | 19.38            |
| (35., 70., 2409.8)                          | RF             | 0.76                      | 12.77         | 10.57            |
|   | K-NN           | <b>0.83</b>               | 12.89         | 10.37            |
|   | SVR            | 0.59                      | 18.95         | 16.02            |
|   | LR             | 0.75                      | 13.14         | 10.23            |
|   | MLP            | 0.82                      | 11.55         | 8.89             |
| (35, 72.5, 2256.2)                          | RF             | <b>0.75</b>               | 20.66         | 16.92            |
|   | K-NN           | 0.67                      | 21.63         | 18.54            |
|   | SVR            | 0.59                      | 26.32         | 20.95            |
|   | LR             | 0.66                      | 23.63         | 17               |
|   | MLP            | 0.38                      | 33.94         | 17.87            |
| (35., 75., 3590.8)                          | RF             | <b>0.55</b>               | 16.93         | 10.13            |
|   | K-NN           | 0.25                      | 19.65         | 14.31            |
|   | SVR            | 0.17                      | 16.33         | 13.81            |
|   | LR             | 0.51                      | 16.1          | 12.05            |
|   | MLP            | 0.24                      | 17.39         | 12.45            |
| (35., 77.5, 4892.9)                         | RF             | 0.4                       | 9.27          | 6.8              |
|   | K-NN           | 0.49                      | 8.68          | 6.61             |
|   | SVR            | 0.4                       | 8.32          | 7.76             |
|   | LR             | <b>0.53</b>               | 8.88          | 6.2              |
|   | MLP            | 0.09                      | 77.02         | 12.12            |

TABLE II: Comparison between different machine learning models in terms of pearson correlation coefficient, mean absolute error (MAE) and standard Deviation of error of the predicted precipitation rate.

| Coordinate (lon, lat, elev) of the index point | Top 10 Features  |
|--|--|
| (27.5, 67.5, 472.9)                            | $rh^{l_1, l_3, l_5}, ar^{l_{12}}, vw^{l_4, l_5, l_{12}}, sh^{l_6, l_7}, uw^{l_4}$          |
| (30., 67.5, 1232.5)                            | $rh^{l_1, l_4, l_5, l_6}, ar^{l_{11}}, vw^{l_1, l_{12}}, sh^{l_7}, uw^{l_1, l_4}$          |
| (30., 70., 721.5)                              | $rh^{l_1, l_4, l_7}, vw^{l_4, l_{14}, l_{15}, l_{16}}, sh^{l_1, l_7}, uw^{l_4}$            |
| (30., 72.5, 148.2)                             | $rh^{l_1, l_4}, vw^{l_{12}, l_{16}}, sh^{l_6, l_7}, uw^{l_2, l_3, l_4}, hg^{l_5}$          |
| (32.5, 70., 1203.)                             | $rh^{l_1, l_8}, ar^{l_{11}}, vw^{l_1, l_4, l_{15}, l_{16}, l_{17}}, sh^{l_1}, uw^{l_1}$    |
| (32.5, 72.5, 326.4)                            | $rh^{l_1, l_2}, ar^{l_1, l_{13}, l_{16}}, vw^{l_1, l_{15}}, sh^{l_1}, uw^{l_4, l_5}$       |
| (32.5, 75., 967.7)                             | $rh^{l_1, l_7, l_8}, ar^{l_{11}, l_{17}}, vw^{l_7}, sh^{l_1}, uw^{l_4, l_5}, hg^{l_5}$     |
| (32.5, 77.5, 4044.4)                           | $rh^{l_1, l_5, l_6, l_8}, ar^{l_{11}, l_{17}}, vw^{l_6, l_7}, uw^{l_6}, hg^{l_5}$          |
| (32.5, 80., 4882.1)                            | $rh^{l_1, l_7, l_8}, ar^{l_{13}, l_{14}, l_{17}}, vw^{l_7, l_{13}}, sh^{l_8}, hg^{l_5}$    |
| (35., 70., 2409.8)                             | $rh^{l_1, l_4, l_5, l_8}, ar^{l_{11}, l_{15}}, vw^{l_1, l_{16}}, uw^{l_1, l_4}$            |
| (35, 72.5, 2256.2)                             | $rh^{l_8}, ar^{l_1, l_7}, vw^{l_{13}, l_{15}, l_{17}}, sh^{l_6}, uw^{l_1, l_4, l_5}$       |
| (35., 75., 3590.8)                             | $rh^{l_1, l_5, l_8}, ar^{l_{11}, l_{17}}, vw^{l_7, l_{13}, l_{16}, l_{17}}, sh^{l_7}$      |
| (35., 77.5, 4892.9)                            | $rh^{l_8}, ar^{l_{11}, l_{15}, l_{16}, l_{17}}, vw^{l_6, l_7, l_{16}}, uw^{l_1}, hg^{l_4}$ |

TABLE III: Top ten contributive predictors for precipitation prediction.

| Feature Name  | Frequency of Occurrence |
|---------------|-------------------------|
| $rh^{l_1}$    | 11                      |
| $rh^{l_8}$    | 8                       |
| $uw^{l_4}$    | 8                       |
| $ar^{l_{11}}$ | 7                       |
| $ar^{l_{17}}$ | 6                       |
| $vw^{l_1}$    | 6                       |
| $rh^{l_5}$    | 5                       |
| $sh^{l_7}$    | 5                       |
| $uw^{l_1}$    | 5                       |
| $vw^{l_7}$    | 5                       |
| $hg^{l_5}$    | 4                       |
| $rh^{l_4}$    | 4                       |
| $sh^{l_1}$    | 4                       |
| $vw^{l_1}$    | 4                       |
| $vw^{l_{15}}$ | 4                       |
| $rh^{l_7}$    | 3                       |
| $sh^{l_6}$    | 3                       |
| $uw^{l_5}$    | 3                       |
| $vw^{l_4}$    | 3                       |
| $vw^{l_{12}}$ | 3                       |
| $vw^{l_{13}}$ | 3                       |
| $vw^{l_{17}}$ | 3                       |
| $ar^{l_1}$    | 2                       |
| $ar^{l_{13}}$ | 2                       |
| $ar^{l_{15}}$ | 2                       |
| $ar^{l_{16}}$ | 2                       |
| $rh^{l_6}$    | 2                       |
| $vw^{l_6}$    | 1                       |
| $ar^{l_{12}}$ | 1                       |
| $ar^{l_{14}}$ | 1                       |
| $hg^{l_4}$    | 1                       |
| $rh^{l_2}$    | 1                       |
| $rh^{l_3}$    | 1                       |
| $sh^{l_8}$    | 1                       |
| $uw^{l_2}$    | 1                       |
| $uw^{l_3}$    | 1                       |
| $uw^{l_6}$    | 1                       |
| $vw^{l_5}$    | 1                       |
| $vw^{l_6}$    | 14                      |

TABLE IV: The frequency of selection of each feature as the top ten contributive predictors towards precipitation prediction.